Strongly coupled evenly divided disks: a new compact and tunable platform for plasmonic Fano resonances

Shi Zhang[1], Xupeng Zhu[2], Wei Xiao[3,4], Huimin Shi[5], Yasi Wang[1], Zhiquan Chen[1], Yiqin Chen[1], Kai Sun[3], Otto L. Muskens[3], C. H. de Groot[4], Shao-Ding Liu[6], Huigao Duan[1, *]

[1]College of Mechanical and Vehicle Engineering, Hunan university, Changsha, 410082, People's Republic of China

[2]School of Physics Science and Technology, Lingnan Normal University, Zhanjiang 524048, People's Republic of China

[3]School of Physics and Astronomy, Faculty of Engineering and Physical Sciences, University of Southampton, Southampton SO17 1BJ, United Kingdom

[4]School of Electronics and Computer Science, Faculty of Engineering and Physical Sciences, University of Southampton, Southampton SO17 1BJ, United Kingdom

[5]Center for Research on Leading Technology of Special Equipment, School of Mecha nical and Electric Engineering, Guangzhou University, Guangzhou 510006, People's Republic of China

[6]Department of Physics and Optoelectronics, Taiyuan University of Technology, Taiyuan 030024, People's Republic of China

*Corresponding author: duanhg@hnu.edu.cn

Abstract

Plasmonic artificial molecules are promising platforms for linear and nonlinear

optical modulation at various regimes including the visible, infrared and terahertz bands. Fano resonances in plasmonic artificial structures are widely used for controlling spectral lineshapes and tailoring of near-field and far-field optical response. Generation of a strong Fano resonance usually relies on strong plasmon coupling in densely packed plasmonic structures. Challenges in reproducible fabrication using conventional lithography significantly hinders the exploration of novel plasmonic nanostructures for strong Fano resonance. In this work, we propose a new class of plasmonic molecules with symmetric structure for Fano resonances, named evenly divided disk, which shows a strong Fano resonance due to the interference between a subradiant anti-bonding mode and a superradiant bonding mode. We successfully fabricated evenly divided disk structures with high reproducibility and with sub-20-nm gaps, using our recently developed sketch and peel lithography technique. The experimental spectra agree well with the calculated response, indicating the robustness of the Fano resonance for the evenly divided disk geometry. Control experiments reveal that the strength of the Fano resonance gradually increases when increasing the number of split parts on the disk from 3 to 8 individual segments. The Fano-resonant plasmonic molecules that can also be reliably defined by our unique fabrication approach open up new avenues for application and provide insight into the design of artificial molecules for controlling light-matter interactions.

Key words: artificial molecules, “sketch and peel” lithography, tiny gap, plasmon coupling, Fano resonance.

1. Introduction

Artificial plasmonic molecules consisting of arranged clusters of plasmonic nanoparticles, have been widely reported due to their ability to interact strongly with incident light and confine electromagnetic energy into small nanometer-sized gaps[1, 2]. Therefore these metallic plasmonic structures have been widely used as promising platforms for sensing[3-5], imaging[6] *etc.* from visible to terahertz regime. The Fano resonance is a phenomenon that is caused by the coupling of a discrete localized state and a continuum of states. Originally introduced in quantum systems, it is also found in many classical systems such as plasmonic artificial molecules. The Fano resonance in plasmonic artificial molecules is always induced by symmetry breaking of the structure [7-10], which introduces the interactions of plasmonic dark modes and bright modes. The destructive interference between subradiant dark plasmon mode and superradiant bright mode can effectively suppress the radiative damping, narrow the resonance linewidth and enhance near field intensity. These properties have attracted much attention in past decades. Many kinds of metallic nanostructures have been reported to support Fano resonance, such as ring/disk cavity[7, 9, 11], nano-shell[12-14], split ring[15-17], dolmen[18-20] and oligomers,[21-27] for practical applications such as surface enhanced infrared absorption [28-30], surface enhanced Raman scattering [31, 32] and enhanced second harmonic generation [33-37] and third harmonic generation[19].

The manipulation of the Fano resonance often depends critically on size or geometry of the structures. Varying the dimensions and geometry allows tuning of the resonance wavelength of the Fano lineshape as well as enhancing the coupling strength

of the superradiant plasmon mode and the subradiant mode. For example, Lassiter *et al.* [38] showed how the Fano resonance in a plasmonic heptamer is influenced by the dimensions and geometry of the structure. In other studies, Liu *et al.* demonstrated that the width of the gap between particles plays a key role for the formation of strong plasmonic Fano resonance [39], and it is very important to fabricate plasmonic nanoparticle oligomer clusters with tiny gaps, where several strong hot-spots can be excited with the formation of Fano resonances, and it can be very useful to improve the performances for the above mentioned applications. However, it is challenging to reliably fabricate oligomer clusters with very tiny gaps using conventional lithography methods[40], and the optical responses for oligomer clusters composed of nanospheres or nanodisks would be strongly affected with the variations of the very tiny gaps.

Here, we design and fabricate a new family of cluster-like evenly divided disk structure (EDD) with narrow gaps using our developed "sketch and peel" lithography (SPL) method, as shown in Figure 1(a)[41]. The EDD structures are subwavelength, with a diameter which is 2-3 times smaller than their resonance wavelength. We systematically investigate the optical response of EDD structures which are divided into different number (EDD-*N*) of parts. The measured and simulated results show that strong Fano resonance could be supported in single EDD structures, and the position and intensity of Fano resonance can be tuned by changing the number of parts *N*. Further calculated charge distributions reveal that both a ring-like satellite dipolar mode (D_R) and a dipolar mode at the center of disk (D_D) can be supported in EDDs. The plasmonic Fano resonance is resulting from the interference of the superradiant bonding

mode and the subradiant anti-bonding mode generated by the hybridization of mode D_R and mode D_D. With the increasing of number *N*, the modulation depth of Fano resonance in this structure is dramatically increased, and strong maximum near field enhancement factor is obtained at position of Fano dip of EDD-8 with about 20 nm gaps. The designed EDD structures provide more degree of freedom to modulate plasmonic structures' optical response and compact integration in practical application.

2. Experimental sections

2.1 Fabrication concept

Figure 1(a) shows the schematic of the individual EDD structure (EDD-8) on the quartz substrate. The radius of the disk *r* is fixed to be 500 nm, and the width of the gap should be small to enhance the plasmonic coupling strength between segments. In this structure, the width of gap is fixed to be 20 nm, and the thickness of the disk *t* is 30 nm. To obtain the designed structure, the "sketch and peel" lithography method is used to fabricate EDD structure arrays. Figure 1(b) shows the fabrication processes of the evenly separated disk by "sketch and peel" lithography method. Firstly, a hydrogen silsesquioxane (HSQ) resist layer was spin coated onto a quartz substrate. The outline and gaps of the structure were exposed by focused electron beam and developed in developer solution. After exposing and developing, the HSQ template was obtained. Subsequently a gold film was evaporated onto the template. The parts of the gold film that are deposited on top of the template and outside the template can be selectively peeled off by using an adhesive polymer, resulting in the final structure as shown in Figure 1b. We note that the HSQ template could not be removed by the adhesive

polymer, therefore the 20-nm width HSQ template which fill the gap and define the outer edge of the disk is not removed. This exposed HSQ template can be eliminated at a later stage by using HF acid if it is desired for practical applications. In our current optical study, the HSQ templates are not removed as it is optically transparent in the near infrared region.

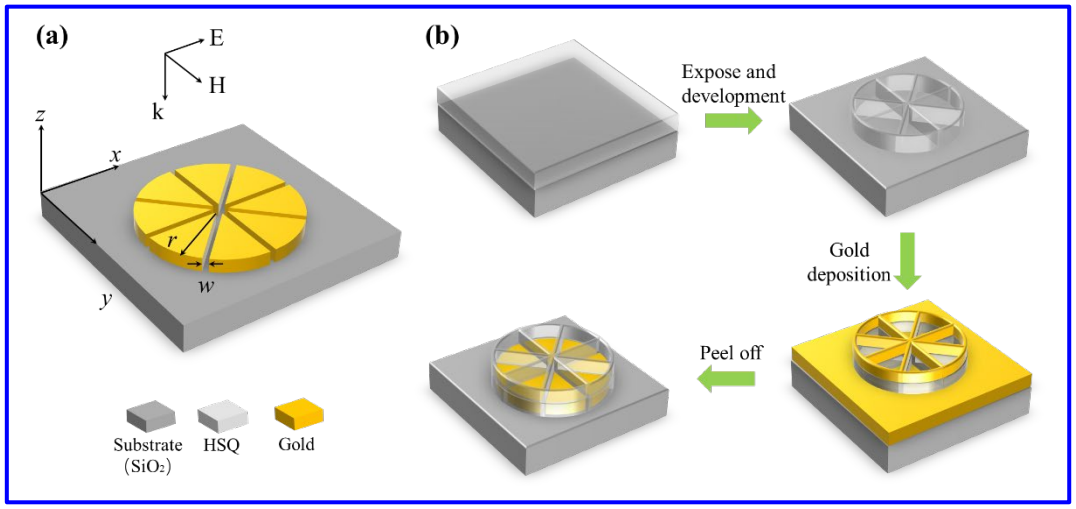

Figure 1. (a) 3D schematic of evenly divided disk (EDD). (b) Fabrication processes of evenly separated disk with the SPL method.

2.2 Electron-beam lithography

All samples were fabricated using an electron beam lithography system (Raith 150TWO). The quartz substrates were ultrasonically rinsed in acetone and isopropanol (IPA) for 10 min, respectively. Then, a hydrogen silsesquioxane (HSQ, XR-1541-006, Dow Corning) resist film with thickness of 100 nm was spin-coated on the quartz substrate with 4000rpm. Conductive polymer layer (Espacer 300Z, Showa Denko K.K.) was spin-coated above the HSQ layer to mitigate the charging effect. Single-pixel outline exposure was conducted by the Raith 150TWO EBL system with an acceleration voltage of 30 kV to define HSQ templates. The lithographic line dose was

set to10000 pC/cm. After the exposure, the sample was rinsed in deionized water to remove the conductive polymer layer and then developed by salty developer (1% NaOH + 4% NaCl) for 1 min. After rinsing the sample in deionized water for 1 min to remove salt residue, the sample was quickly transferred into IPA for 30 s to decrease the surface tension and finally dried by N_2 flow.

2.3 Metal deposition and lift-off

A 30-nm-thick gold layer was deposited onto the samples by thermal evaporator (JSD300, Anhui Jiashuo Vacuum Technology Co. Ltd) with a deposition rate of 1Å/sec. After metallization, optical adhesive (NOA-61, Norland Products Inc.) was poured onto the sample and cured under the illumination of ultraviolet for 20 min. Finally, the target structures were obtained after selective peeling process.

2.4 Scanning electron microscopy metrology

The SEM images of metallic nanostructures were acquired by a field-emission scanning electron microscope (Sigma HD, Carl Zeiss) with an accelerating voltage of 2 kV and a working distance of 6.9 mm.

2.5 Optical characterization

The polarization-resolved extinction spectra (1-transmittance) of all samples were collected by a Fourier transform infrared microscope (Thermo-Nicolet Nexus 670) system equipped with an optical objective (Cassegrain, ×15, 0.2 NA) and MCT-A detector. The transmittance spectra were normalized with respect to the transmittance through a quartz substrate.

2.6 Electromagnetic simulation

Finite-difference time-domain method was employed to calculate the extinction spectra and the corresponding charge and near-field distributions at feature position with a commercial software (Lumerical Solutions). Total-field scattered-field source is employed to simulate the scattering cross section and absorption cross section. The extinction spectrum is given by the sum of scattering and absorption spectrum. Perfectly matched layer (PML) boundary conditions were used for the three dimensions and a mesh size of 2.5 nm for the structure region was utilized. The dielectric constant of Au was based on the database of Palik, and the exposed HSQ was replaced by SiO_2 (Palik).

3. Results and discussion

3.1 Fabrication results

Scanning electron microscopy (SEM) images of the fabricated sample are shown in Figure 2. Figure 2(a) presents an array of EDDs and demonstrates that the sample can be fabricated uniformly over a large area by using the SPL method. The pitch of the array is fixed at 2 μm. Figures 2(b) and (c) show higher magnification SEM images of a randomly selective area. It can be clearly observed that the gaps are well defined and have a width of around 20 nm. The HSQ template provides an effective separation disconnecting the segments of the disk preventing any conductive coupling. Only slight deviations from the design are seen toward the center of the disk, where the definition of the tips is somewhat affected by the dimensions of the HSQ template.

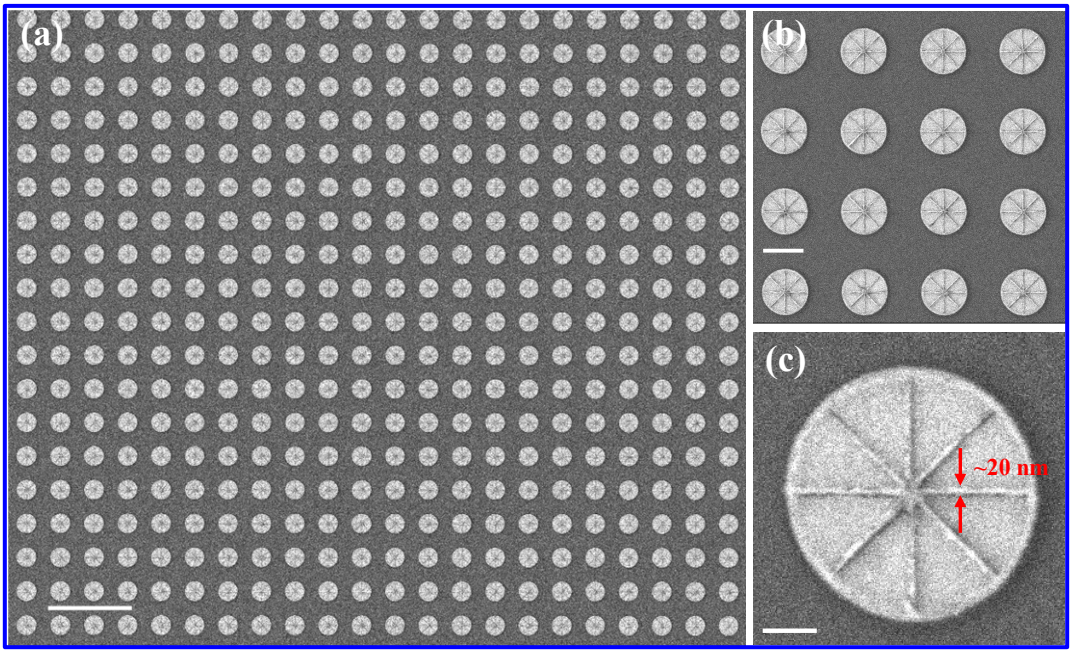

Figure 2. SEM images of the fabricated evenly separated disk array (a), random selected enlarged area (b) and individual EDD structure (c). The length of scale bar is 5 μm, 1 μm, 250 nm, respectively

3.2 Optical behavior and mode analysis

To investigate the optical behavior of disks divided into different number of parts, the extinction spectra (1-transmittance) of EDDs with different N ranging from 3 to 8 were measured using Fourier transform infrared (FTIR) system. All measured structures were prepared in square arrays of 150 μm×150 μm with the pitch of 2 μm. The transmittance spectra were based on the measured intensity of the transmitted light from the single patch of nanostructure array (I) and the bare quartz substrate with the same area size as the array (I_0), and the transmittance spectra T were obtained by normalization as $T \propto I/I_0$. Figure 3(a) shows the measured extinction spectra of EDDs arrays with different N under normal incidence. For EDD-3 structure (black line), there is only one prominent peak centered at around 2.5 μm. The optical response of EDD-4

(red line) also displays one blue-shifted prominent peak compared with EDD-3. When *N* increases to 5 (blue line), a small dip centered appears at around 2.3 μm, splitting into two peaks. The position of dip is gradually blueshifted and the dip becomes more apparent as *N* further increases to 8. The corresponding SEM images of prepared EDD structures with different *N* are shown in Figure 3 (b). Figure 3 (c) represents simulated extinction spectra for the corresponding structures as in experiment. It is obvious that simulated results are agree well with experiment results, excepting for a small dip appear in simulated extinction spectra of EDD-3 and EDD-4, resulting from the weak coupling between different modes in EDD-3 and EDD-4. We also investigated the effect of the polarization angle of the incident light on the spectra. As the change of the polarization angle of the incident light, the extinction spectra show no obvious changes (see supplementary Figure S1), indicating that the effect of incident polarization on the Fano behaviors in our designed structure is ignorable.

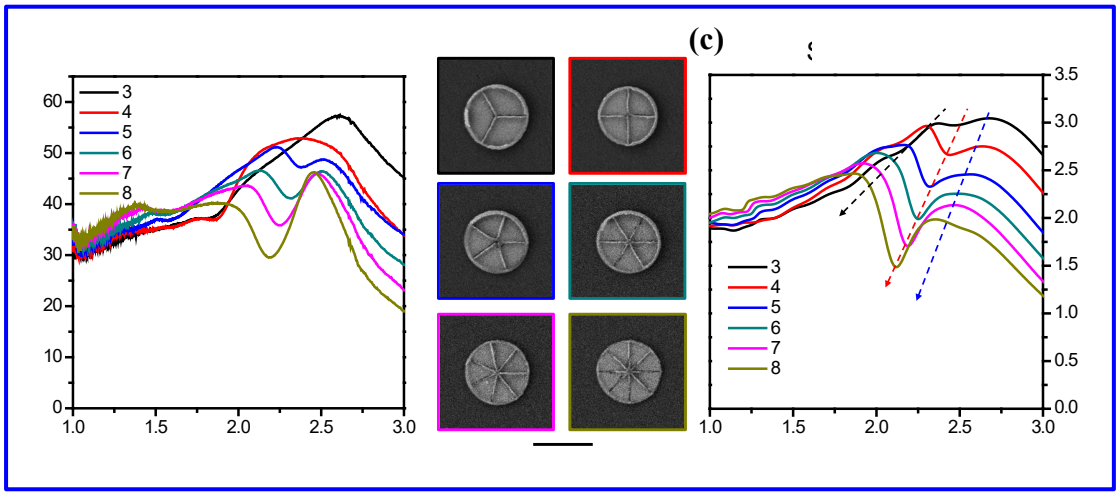

Figure 3. (a) Measured extinction spectra (1-transmittance) of EDDs arrays with different N. (b) Representative SEM images of the corresponding structures. (c) Corresponding simulated extinction spectra.

To understand the nature of observed extinction feature in Figure 3, we further analyzed the plasmon hybridization scheme though calculations of the charge distributions and near field enhancement distributions with the incident polarization along *x*-axis. Figure 4(a) presents the simulated extinction spectrum of EDD-8. The spectral feature positions are labeled as positions P_1-P_4. In EDD-8 structures, under the excitation of polarized incident light, the charges could be gathered at the edge of the gaps, formed a ring-like satellite dipolar mode (D_R) or charges are gathered in the center of disk, formed a center dipolar mode (D_D), as shown in Figure 4(b). The interaction between D_R mode and D_D mode leads to the formation of an anti-bonding mode D_{AB} and a bonding mode D_B. The generation of the Fano dip is induced by interference of the anti-bonding D_{AB} mode and the bonding mode D_B. It is noted that the plasmon modes of EDD-8 are similar to the plasmon mode in heptamer, but have very different causes. The plasmon mode in the heptamer is considered as the interaction of the plasmon mode of a hexamer and that of a monomer, liking satellite dipolar mode D_R and center dipolar mode D_D in EDD. However, the hexamer that supports satellite dipolar modes and the monomer that support central dipolar mode in the heptamer structure are independent, whereas the mode D_R and mode D_D are supported by the gaps in EDD structure at different excitation wavelengths, it's a collective effect of all segments of the structure. Therefore, compared with oligomers, EDD structures allow more compact on-chip integration and more convenient geometry-tuning, which are of great importance in many applications.

To verify our analysis, the corresponding charge distributions (upper panels) and

near field enhancement distributions (lower panel) are shown in Figure 4(c). The charge distribution at position P_1 reveals that the optical properties of EDD-8 at position P_1 is dominated by six ring-like satellite dipoles, i.e. mode D_R, which is similar to the in-phase collective dipolar mode in hexamer. The charge distribution around position P_3 shows that charges are mostly concentrated in the center of the structure, i.e. D_D mode. The charge distributions at position P_2 and P_4 demonstrated the formation of the anti-bonding mode D_{AB} and the bonding mode D_B. The corresponding near-field enhancement distributions at each panel position are shown in lower panels of Figure 4(c). The numbers at the lower left corner of each figure are the maximum near-field enhancement factors at each labeled position, demonstrating that maximum field enhancement can be obtained at position P_2 due to the suppression of radiation damping.

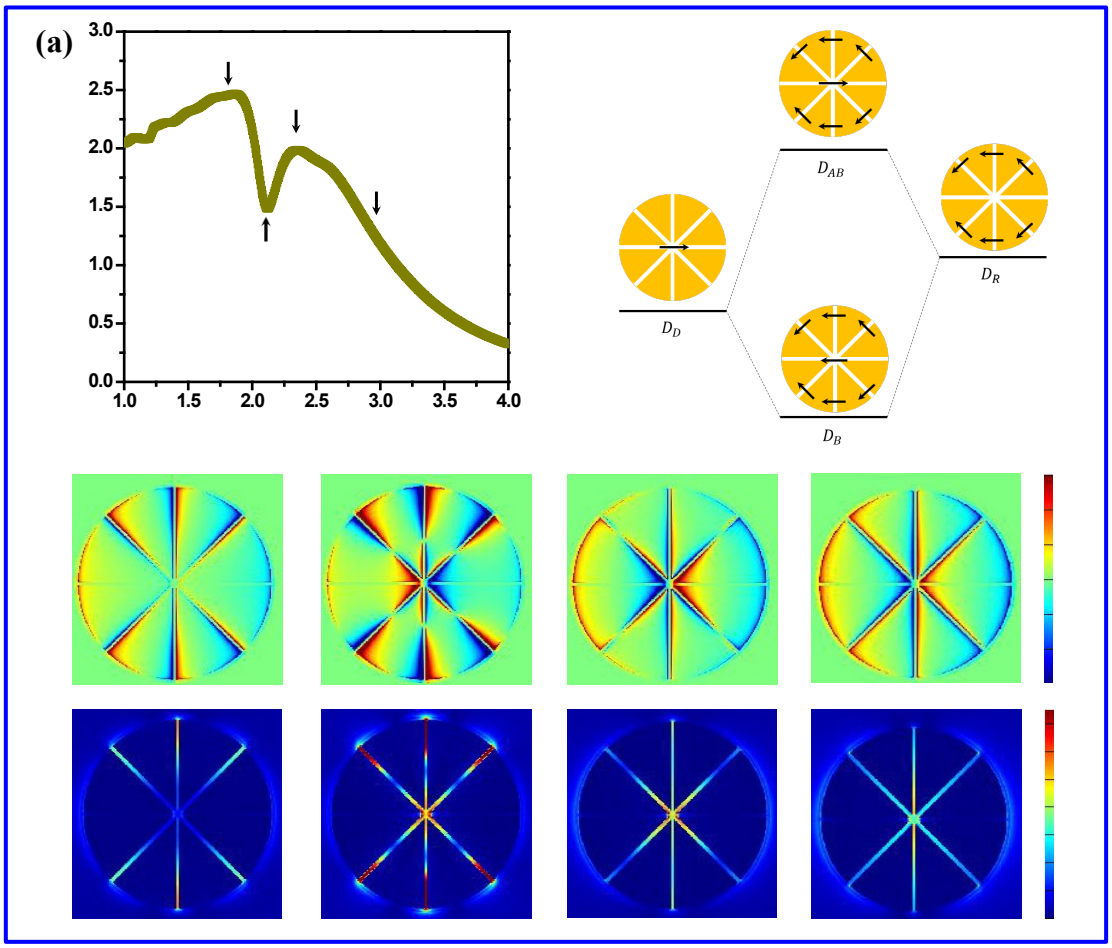

Figure 4. Plasmon resonance mode analysis. (a) Measured and calculated extinction of EDD (N = 8) structure with incident polarization along x-axis. (b) The hybridization schemes of the EDD (N = 8) structure. The black arrows represent the direction of dipole. (c) The charge distribution (upper panel) and near field enhancement E/E_0 (lower panel) at each labeled position.

Other EDD structures (N=3-7) have a similar plasmon hybridization scheme. Figure 5(a-c) demonstrates the near field enhancement distributions and charge distributions of EDD (N=3-7) at spectral feature positions, i.e. positions 1-3 in Figure 3(c). The incident polarizations are all along one of the gaps. The first left column of Figure 5(a-c) reveals the charge distributions and near field enhancement distributions of EDD-3. At position 1 a plasmon mode similar to D_R can be observed, but only have two ring-like satellite dipoles. The charge distribution at position 2 does not show a

significant difference with position 1. Bonding D_D mode is seen at position 3. From the charge distribution of EDD-3 at each spectral feature position we can see that three modes cannot be clearly distinguished, and the coupling between mode D_R and mode D_D is weak. Therefore, the Fano dip in the extinction spectrum of EDD-3 in Figure 3 is not obvious. EDD-4 has a similar plasmon mode as EDD-3, but the two satellite dipoles of the mode D_R are now symmetrically arranged. The coupling strength of mode D_R and mode D_D is increased compared with EDD-3 and the near-field enhancement is higher than that of EDD-3. When *N* increases to more than 5, the D_R mode, D_D mode and D_{AB} mode can be clearly distinguished from charge distributions at three spectral feature positions. In addition, as the number *N* increases, the distance between the satellite dipoles becomes smaller, which causes the higher energy of D_{AB} mode, leading to the blue shift of the Fano dip. These results proved that our analysis in Figure 4 is still applicable in other EDDs structures. The cause of Fano resonance in EDD-*N* (*N* = 3-7) is the same as EDD-8. Note that the generation of the Fano resonance is the synergy effect of all segments of the EDD structure, if some segments of the EDD structure are removed, fixing the polarization of incident light along the direction shown in FigureS2(a), the coupling of the subradiant mode superradiant mode is weaken and the intensity of the Fano resonance reduced. When the polarization of the incident light is perpendicular to the previous excitation direction, the excited mode is completely different, the Fano resonance disappears, the optical response of the EDD-8 is dominated by the magnetic resonance. (see supplementary Figure S2).

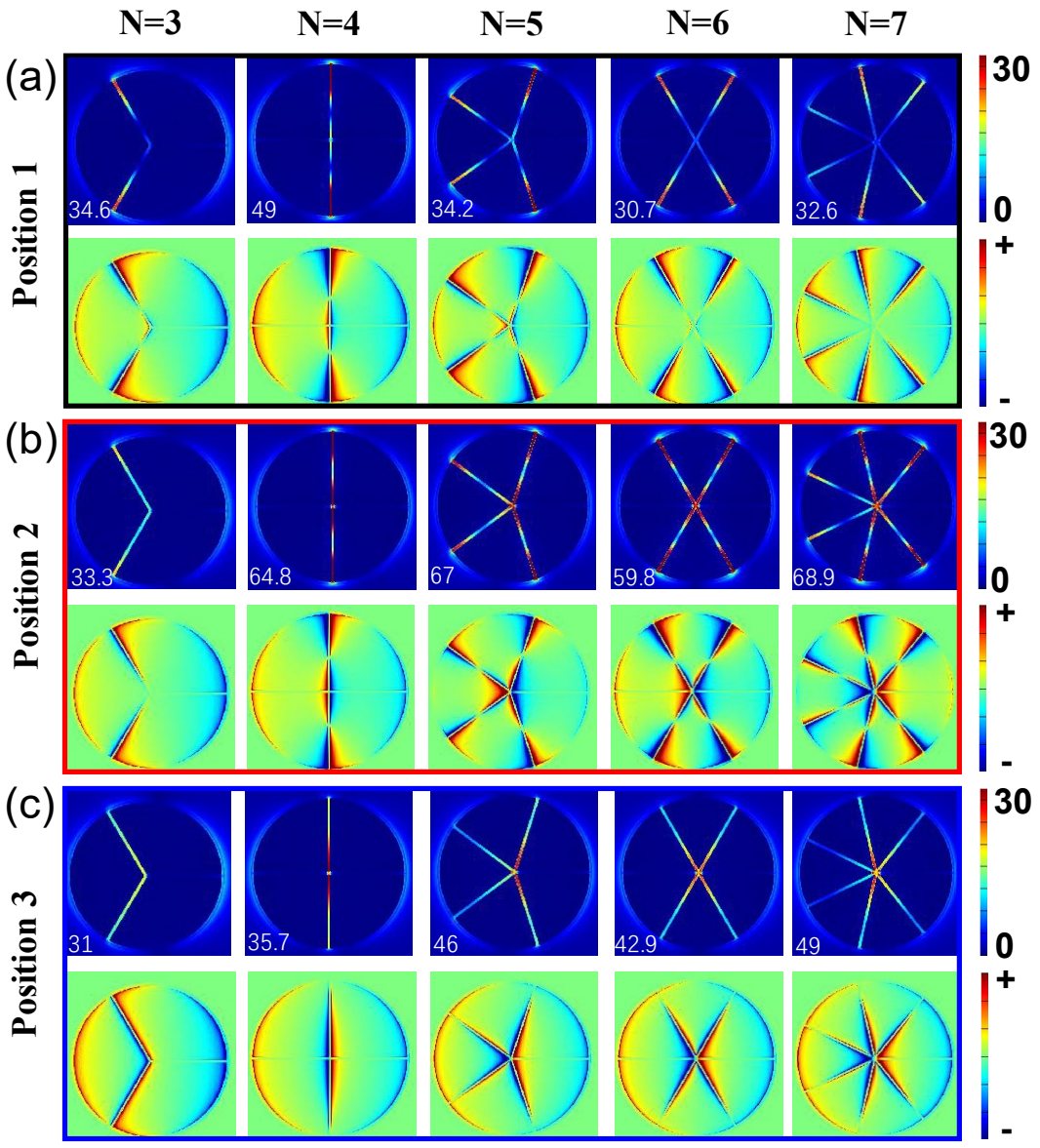

Figure 5. Field enhancement distributions and charge distributions of EDD structures with different *N* (3-7) at each spectral feature position in Figure 3(c): (a-c) each structures' field enhancement distributions and charge distributions corresponding to position 1, position 2 and position 3 in Figure 3(c), respectively. The numbers at the lower left corner of each figure are the maximum near-field enhancement factors at each position. All the charge distributions and near field distributions use the same color bar.

3.3 Effects of disk radius and gap size

The spectral modulation depth is of great importance in many practical applications. The modulation depth of Fano resonance is dominated by the net dipole moment of the subradiant mode. The smaller the net dipole moment, the greater the modulation depth. In EDD structures, for the subradiant D_{AB} mode, the net dipole of the ring-like satellite diploes oscillates oppositely with the central dipole. Since the net dipole moment of the subradiant mode depends on the dipole moment of central dipole and ring-like satellite dipoles. We can enhance the modulation depth of Fano dip by making the dipole moment of central dipole and ring-like satellite dipoles more perfectly balanced. Figure 6(a) shows the extinction spectra of EDDs-8 with various radius under incident polarization perpendicular to one split gap. When *r* is 400 nm, there is a Fano resonance dip around 1.7 μm. By enlarging the disk radius *r*, the position of Fano resonance dip is dramatically redshifted to around 3 μm when *r* is increased to 750 nm. The modulation depth of the Fano dip also shows obviously increase trend with the increase of *r* since the increased dipole moment of central dipole is more balanced with the ring-like satellite dipoles. The coupling strength of destructive interference of D_{AB} and D_B are sufficiently increased, resulting in a deeper Fano dip.

In addition, we also investigated the effects of the gap width on spectra of the EDD structures. Figure 6 (b) shows the extinction spectra of EDD-8 with different gap widths. When the gap width is 80 nm, a weak Fano resonance dip appears at around 1.8 μm.

Then we decrease the width of gap from 80 nm to 10 nm with 10 nm step size. As the gap width *w* decreases, the modulation depth of the Fano dip is increased and the position of Fano dip is simultaneously red shifted. This behavior can be explained by the strong enhancement of the plasmon coupling strength as the gap width is reduced. As a result, the modulation depth of the Fano resonance is also significantly increased. It is noted that the shift of the Fano dip with the decrease of the gap width is nonlinear and therefore a much greater spectral sensitivity to structural parameters is obtained for smaller gap width, which is a result of the dramatically increased coupling strength at small gap width.

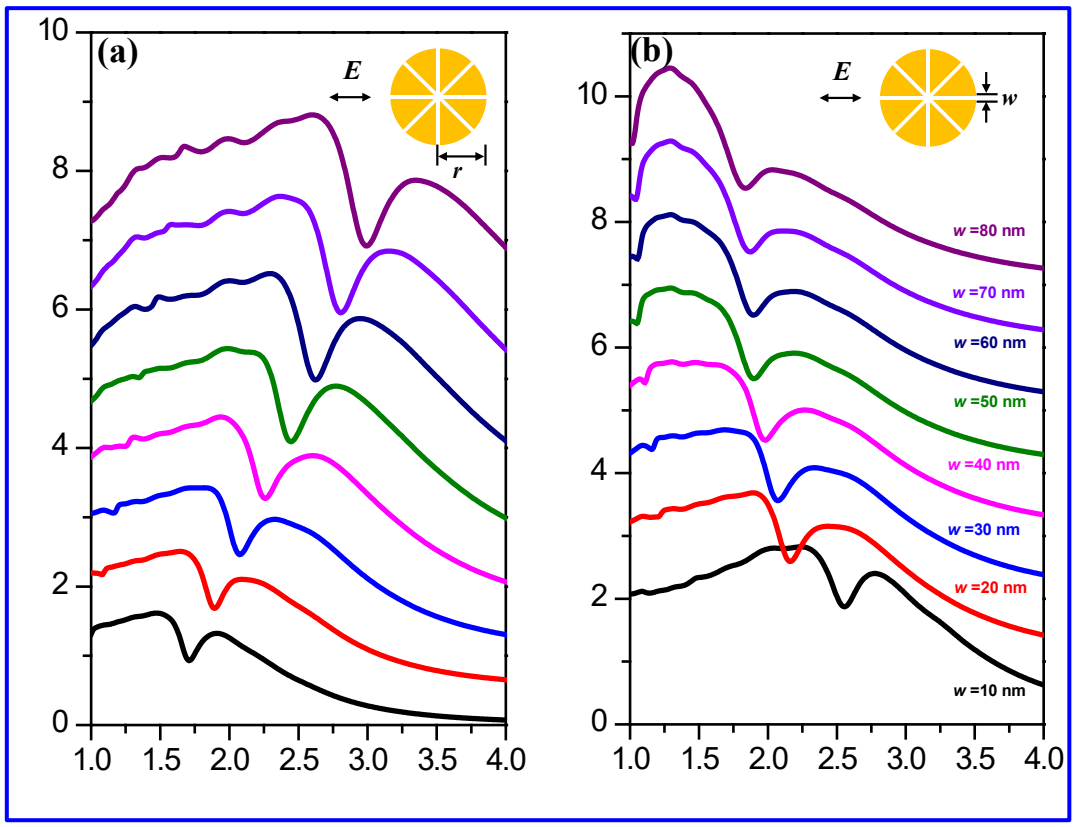

Figure 6. Simulated extinction spectra of EDDs-8 versus the radius of EDDs range from 400 nm to 750 nm (a), and gap width of EDDs range from 15 nm to 80 nm (b). The other parameters are the same with defined in Figure 1.

4. Conclusion

We have successfully designed and fabricated a series of plasmonic structures by evenly dividing a perfect disk. The optical behaviors of the designed EDD structures were systemically investigated. Sketch and peel lithography resulted in high quality structures with gaps of around 20 nm and excellent reproducibility over large areas. We found that a Fano resonance could be supported in the EDD structures. The position of the Fano dip blue shifts and the modulation depth of the Fano resonance is increased by increasing the number of segments *N* of the EDD structures. The simulated charge distributions and near-field enhancement distributions show that Fano resonances are generated due to interference of super- and sub-radiant plasmonic modes, which is similar to the mechanism found in plasmonic particle oligomers. The EDD structures provide an additional degree of freedom to modulate plasmon resonance. Besides, the highly confined energy in tiny gaps of EDDs may be highly useful in practical applications such as surface enhanced Raman scattering, surface enhanced infrared absorption, refractive sensing, and high order harmonic generation.

Acknowledgments

We gratefully acknowledge financial support from the National Natural Science Foundation of China (Grant nos. 51722503, 51621004, 51805160, 11574078 and 6171101530), Royal Society-Newton Mobility (Grant IEC\NSFC\170193) and Science and Technology Bureau Foundation of Changsha City (kh1904005), State Key Laboratory Open Fund 31715004.

Conflict of Interest

The authors declare no conflict of interest.

Reference

[1] Wang H, Brandl D W, Nordlander P and Halas N J 2007 *Accounts of Chemical Research* 40 53

[2] Haran G and Chuntonov L 2018 *Chem. Rev.* 118 5539

[3] Liu N, Tang M L, Hentschel M, Giessen H and Alivisatos A P 2011 *Nat. Mater.* 10 631

[4] Willets K A and Van Duyne R P 2007 *Annual Review of Physical Chemistry* 58 267

[5] Verellen N, Van Dorpe P, Huang C, Lodewijks K, Vandenbosch G A E, Lagae L and Moshchalkov V V 2011 *Nano Lett.* 11 391

[6] Willets K A, Wilson A J, Sundaresan V and Joshi P B 2017 *Chem. Rev.* 117 7538

[7] Hao F, Sonnefraud Y, Dorpe P V, Maier S A, Halas N J and Nordlander P 2008 *Nano Lett.* 8 3983

[8] Luk'yanchuk B, Zheludev N I, Maier S A, Halas N J, Nordlander P, Giessen H and Chong C T 2010 *Nat. Mater.* 9 707

[9] Hao F, Nordlander P, Sonnefraud Y, Dorpe P V and Maier S A 2009 *ACS Nano* 3 643

[10] Limonov M F, Rybin M V, Poddubny A N and Kivshar Y S 2017 *Nat. Photon.* 11 543

[11] Cetin A E and Altug H 2012 *ACS Nano* 6 9989

[12] Hu Y, Noelck S J and Drezek R A 2010 *ACS Nano* 4 1521

[13] Mukherjee S, Sobhani H, Lassiter J B, Bardhan R, Nordlander P and Halas N J 2010 *Nano Lett.* 10 2694

[14] Wu D, Jiang S and Liu X 2011 *The Journal of Physical Chemistry C* 115 23797

[15] Manjappa M, Srivastava Y K, Cong L, Al-Naib I and Singh R 2017 *Adv. Mater.* 29 1603355

[16] Liu S-D, Yang Z, Liu R-P and Li X-Y 2012 *ACS Nano* 6 6260

[17] Bao Y, Hu Z, Li Z, Zhu X and Fang Z 2015 *Small* 11 2177

[18] Verellen N, Sonnefraud Y, Sobhani H, Hao F, Moshchalkov V V, Dorpe P V, Nordlander P and Maier S A 2009 *Nano Lett.* 9 1663

[19] Metzger B, Schumacher T, Hentschel M, Lippitz M and Giessen H 2014 *ACS Photonics* 1 471

[20] Yan C and Martin O J F 2014 *ACS Nano* 8 11860

[21] Hentschel M, Dregely D, Vogelgesang R, Giessen H and Liu N 2011 *ACS Nano* 5 2042

[22] Alegret J, Rindzevicius T, Pakizeh T, Alaverdyan Y, Gunnarsson L and Käll M 2008 *The Journal of Physical Chemistry C* 112 14313

[23] Chuntonov L and Haran G 2011 *Nano Lett.* 11 2440

[24] Hao E and Schatz G C 2003 *The Journal of Chemical Physics* 120 357

[25] Nordlander P, Oubre C, Prodan E, Li K and Stockman M I 2004 *Nano Lett.* 4 899

[26] Yorulmaz M, Hoggard A, Zhao H, Wen F, Chang W-S, Halas N J, Nordlander P and Link S 2016 *Nano Lett.* 16 6497

[27] Liu N, Mukherjee S, Bao K, Brown L V, Dorfmüller J, Nordlander P and Halas N J 2012 *Nano Lett.* 12 364
[28] Neubrech F, Huck C, Weber K, Pucci A and Giessen H 2017 *Chem. Rev.* 117 5110
[29] Wu C, Khanikaev A B, Adato R, Arju N, Yanik A A, Altug H and Shvets G 2012 *Nat. Mater.* 11 69
[30] Ishikawa A, Hara S, Tanaka T, Zhang X and Tsuruta K 2017 *Appl. Phys. Lett.* 111 243106
[31] Ye J, Wen F, Sobhani H, Lassiter J B, Van Dorpe P, Nordlander P and Halas N J 2012 *Nano Lett.* 12 1660
[32] Fang W, Jia S, Chao J, Wang L, Duan X, Liu H, Li Q, Zuo X, Wang L, Wang L, Liu N and Fan C 2019 *Science Advances* 5 eaau4506
[33] Zhang S, Li G-C, Chen Y, Zhu X, Liu S-D, Lei D Y and Duan H 2016 *ACS Nano* 10 11105
[34] Liu S-D, Leong E S P, Li G-C, Hou Y, Deng J, Teng J H, Ong H C and Lei D Y 2016 *ACS Nano* 10 1442
[35] Walsh G F and Dal Negro L 2013 *Nano Lett.* 13 3111
[36] Thyagarajan K, Butet J and Martin O J F 2013 *Nano Lett.* 13 1847
[37] Butet J, Brevet P-F and Martin O J F 2015 *ACS Nano* 9 10545
[38] Lassiter J B, Sobhani H, Fan J A, Kundu J, Capasso F, Nordlander P and Halas N J 2010 *Nano Lett.* 10 3184
[39] Hentschel M, Saliba M, Vogelgesang R, Giessen H, Alivisatos A P and Liu N 2010 *Nano Lett.* 10 2721
[40] Fang F, Zhang N, Guo D, Ehmann K, Cheung B, Liu K and Yamamura K 2019 *International Journal of Extreme Manufacturing* 1 012001
[41] Chen Y, Xiang Q, Li Z, Wang Y, Meng Y and Duan H 2016 *Nano Lett.* 16 3253